



Radio Science

RESEARCH ARTICLE

10.1029/2017RS006499

Key Points:

- Performance evaluation of MIDAS compared with ANNs to reconstruct ionospheric total electron content during geomagnetic storms
- MIDAS performs 13% better than ANNs in African midlatitude region
- ANNs perform 24% better than MIDAS in African low-latitude region

Correspondence to:

J. C. Uwamahoro,
juwamahoro@sansa.org.za

Citation:

Uwamahoro, J. C., Giday, N. M., Habarulema, J. B., Katamzi-Joseph, Z. T., & Seemala, G. K. (2018). Reconstruction of storm-time total electron content using ionospheric tomography and artificial neural networks: A comparative study over the African region. *Radio Science*, 53, 1328–1345. <https://doi.org/10.1029/2017RS006499>

Received 10 NOV 2017

Accepted 11 OCT 2018

Accepted article online 16 OCT 2018

Published online 5 NOV 2018

Reconstruction of Storm-Time Total Electron Content Using Ionospheric Tomography and Artificial Neural Networks: A Comparative Study Over the African Region

Jean Claude Uwamahoro^{1,2,3} , Nigusie M. Giday^{1,2,4}, John Bosco Habarulema^{1,2} , Zama T. Katamzi-Joseph^{1,2}, and Gopi Krishna Seemala⁵ 

¹South African National Space Agency (SANSA), Space Science, Hermanus, South Africa, ²Department of Physics and Electronics, Rhodes University, Grahamstown, South Africa, ³Department of Physics, College of Science and Technology, University of Rwanda, Kigali, Rwanda, ⁴Ethiopian Space Science and Technology Institute (ESSTI), Addis Ababa, Ethiopia, ⁵Indian Institute of Geomagnetism (IIG), Mumbai, India

Abstract The work presented here aims to evaluate the capabilities of Multi-Instrument Data Analysis System (MIDAS) compared with artificial neural networks (ANNs) to reconstruct storm-time total electron content (TEC) over the African low-latitude and midlatitude regions. For MIDAS, the inversion was done based on the Global Positioning System (GPS) measurements from receiver stations extending from -30° to 36° in latitude and 30° to 44° in longitude while for ANNs, individual storm-time models based on historical GPS data from receivers within the same region covered by MIDAS were used. Based on the minimum *Dst* index reached during the storm period, moderate ($-50 \text{ nT} \geq Dst > -100 \text{ nT}$), strong ($-100 \text{ nT} \geq Dst > -200 \text{ nT}$), and severe ($-200 \text{ nT} \geq Dst > -350 \text{ nT}$) storms were used for validation. MIDAS and ANNs results were compared with IRI-2016 predictions and validated with real GPS TEC observations. A statistical analysis revealed that MIDAS and ANNs provide comparable results in storm-time TEC reconstruction with average mean absolute errors of 4.81 and 4.18 TECU respectively. However, MIDAS performed better compared to ANNs in following TEC enhancements and depletions as well as short-term features observed during the selected storm periods. In terms of latitude, it was found that on average, MIDAS performs 13% better than ANNs in the African midlatitude, while ANN model performs 24% better than MIDAS in low latitudes. Furthermore, comparisons with IRI predictions showed that both MIDAS and ANNs produce more accurate estimations of the storm-time TEC than IRI model.

1. Introduction

The ionospheric electron density varies due to a mixture of complex mechanisms that modify temporal and spatial distributions of ionized particles such as changes in solar radiation intensity, interaction of interplanetary and geomagnetic fields, and the atmospheric dynamics (Mitchell & Spencer, 2003). The state of the ionosphere becomes more complicated during geomagnetic storms since the ionospheric electron density is redistributed due to electric field perturbations and induced currents in the ionosphere (Tsurutani et al., 2004, 2006), and other mechanisms such as neutral winds (Fesen et al., 1989), expansion of the equatorial ionisation anomaly (Tsurutani et al., 2004), large-scale traveling ionospheric disturbances (Borries et al., 2009), and neutral composition changes (Prölss, 1980). It is known from the literature that equatorward meridional neutral winds and associated traveling ionospheric disturbances are responsible for positive ionospheric response. At high latitudes, a storm-induced surge in meridional winds forces ionized particles to move upward to a region of lower recombination rate resulting in an increase in electron density and, hence, in total electron content (TEC) (Fuller-Rowell et al., 1994). Another cause of positive ionospheric response is prompt penetration electric field, which lifts dayside equatorial and near-equatorial ionosphere to higher altitudes where the recombination rate is lower (Tsurutani et al., 2004). Enhanced eastward electric field increases the fountain effect (superfountain effect), which can expand towards midlatitude resulting in TEC enhancement (Tsurutani et al., 2004). Conversely, changes in neutral gas composition have been listed among the causes of negative storm effects (Tsurutani et al., 2004). Recent studies have shown that a decrease in TEC observed during midlatitude storms correlated well with a decrease in O/N₂ ratio (Habarulema et al., 2013; Katamzi & Habarulema, 2014).

For the benefits of the scientific community, ionospheric tomography and modeling are of high importance for radio communication and satellite navigation for their role in understanding spatial distribution of the electron concentration and short-term temporal variations in the ionosphere (Chartier et al., 2014; Ercha et al., 2015). The ionospheric TEC and electron concentration are good indicators of the morphology of the ionosphere and can therefore be used for ionospheric studies and satellite applications (Mitchell & Spencer, 2003). There exist a number of studies related to ionospheric tomography imaging based on an inversion algorithm, namely Multi-Instrument Data Analysis System (MIDAS; Chartier et al., 2014; Dear & Mitchell, 2006; Giday et al., 2016; Jayawardena et al., 2016; Materassi & Mitchell, 2005; Meggs et al., 2005; Mitchell & Spencer, 2003; Muella et al., 2011; Rose et al., 2014; Yin et al., 2004). Using data from a network of GPS receivers over the U.S. midlatitudes, it has been proven that MIDAS can produce images of electron concentration and TEC during extreme geomagnetic conditions ($K_p = 9$) that are in good agreement with observations (Yin et al., 2004). The maximum electron density of the F2 layer (NmF_2) and peak height (hmF_2) obtained from MIDAS reconstruction using data from GPS receivers within South Africa have shown good agreement with the ionosonde measurements (Giday et al., 2016). The authors further showed that MIDAS provides more accurate estimates of NmF_2 than IRI model while the reverse was noticed for hmF_2 . With respect to the NmF_2 values extracted from MIDAS reconstruction during geomagnetic storms, it was found that MIDAS performs well for some storms while for others, relatively high deviations were observed (Giday et al., 2016). For the European and North American regions, a good agreement between the reconstructed TEC by MIDAS and IRI with observations was observed despite some discrepancies for some periods of solar activity between 1998 and 2009 (Chartier et al., 2012). MIDAS has also been applied to generate electron density and TEC maps for the equatorial ionosphere over the South America using data from GPS receivers distributed throughout the region of interest (Materassi & Mitchell, 2005). These examples therefore demonstrate that MIDAS has been validated in low-latitude and midlatitude regions.

MIDAS ionospheric tomographic imaging results were mainly focused on the midlatitudes (Chartier et al., 2012; Dear & Mitchell, 2006; Giday et al., 2016; Meggs et al., 2005; Rose et al., 2014; Yin et al., 2004). The few works that are related to ionospheric imaging for the low-latitude region were done for geomagnetically quiet conditions (Chartier et al., 2014; Materassi & Mitchell, 2005; Muella et al., 2011). MIDAS is a general package that provides a time varying 3-D image of the ionosphere. However, the parameters and methods of inversions in the setup of MIDAS need to be fine-tuned and adapted to different latitude regions. Therefore, validating and adapting MIDAS algorithm in the African low latitude and midlatitude is needed so as to offer the space weather community more alternatives to characterize the ionosphere, since the African region has limited research infrastructures and in this case, ground-based Global Navigation Satellite System receivers. This is particularly important for the African low-latitude ionosphere characterized by high TEC gradients (even more pronounced during geomagnetic storms) as result of a mixture of complex electrodynamic mechanisms (Tsurutani et al., 2004), and double transport of ionized particles caused by horizontal neutral winds and fountain effect (Fesen et al., 1989).

On the other hand, artificial neural networks (ANNs) technique has intensively been applied in modeling of some ionospheric parameters such as TEC (Acharya et al., 2011; Leandro & Santos, 2007; Ma et al., 2005; Maruyama, 2007; Ratnam et al., 2012; Tulunay et al., 2004) and ionospheric critical frequency of F2 layer, foF_2 (Cander, 1998; McKinnell & Poole, 2004; Oyeyemi et al., 2006; Poole & McKinnell, 2000). Most of these studies reported a good agreement between the actual data and ANN model predictions. Comparative TEC results in low latitudes showed superior performance of ANN models over the IRI model (Okoh et al., 2016; Watthanasangmechai et al., 2012). A similar observation was reported for the African midlatitude region when evaluating the performance of ANNs and IRI during geomagnetically quiet conditions (Habarulema et al., 2007, 2009) and geomagnetic storms (Habarulema et al., 2010). Recently, when ANN and empirical orthogonal function (EOF) models were applied to storm-time TEC modeling for a midlatitude station (Sutherland [SUTH]: 32.38°S, 20.81°E; South Africa), findings showed that ANN results agree with observations better than EOF predictions (Uwamahoro & Habarulema, 2015). Overall, ANN model has been reported to perform better than other storm-time TEC models such as IRI and EOF (Habarulema et al., 2007, 2009; Okoh et al., 2016; Uwamahoro & Habarulema, 2015; Watthanasangmechai et al., 2012).

Although MIDAS and ANNs have separately been tested under both geomagnetically quiet and disturbed conditions, no study has compared their performances relative to each other over various latitudes (low-latitude and midlatitude regions). In this perspective, the main objective of this paper is to statistically evaluate, for the first time, the capability of MIDAS compared with ANNs to reconstruct storm-time TEC over

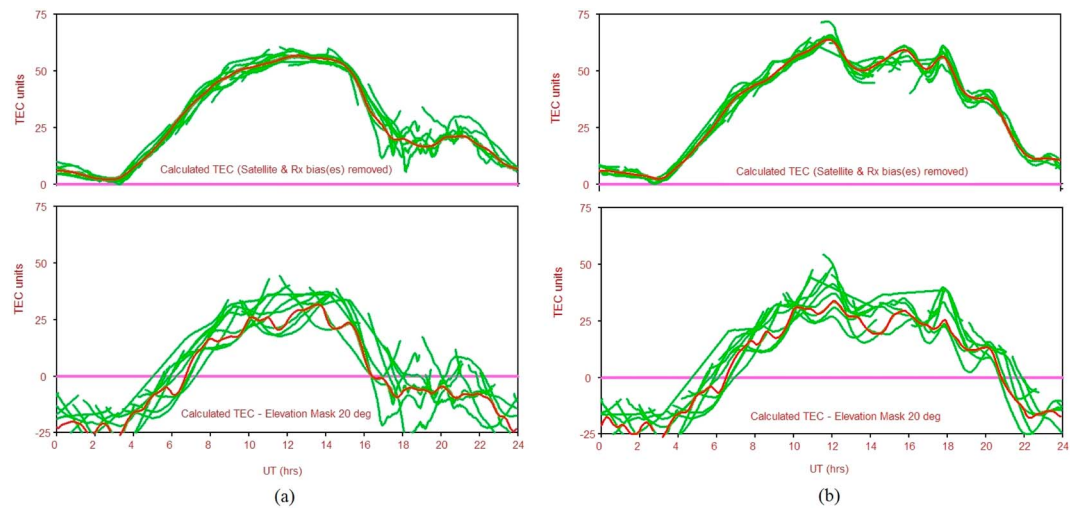


Figure 1. Calibrated (top panels) and uncalibrated (bottom panels) TEC over Nazret (NAZR, 8.57°N, 39.29°E, 0.25°S geomagnetic), by taking into account cycle slips, satellite, and receiver biases for quiet (16 March 2015, Figure 1a) and disturbed (16 March 2015, Figure 1b) days. Red and green lines show the average vertical TEC over all satellites and vertical TEC from individual satellite, respectively. TEC = total electron content.

the African low-latitude and midlatitude regions. Additionally, MIDAS and ANN results are compared with IRI-2016 TEC predictions.

A study like the one presented in the current work, which compares different modeling/reconstructing techniques of the ionospheric TEC during geomagnetic storms, is important for future improvements in ionospheric modeling. Evaluation of how much percentage and under which circumstances a model is more accurate with respect to another is a contribution towards the efforts that should be made to implement a more efficient optimization algorithm for storm-time TEC modeling/reconstruction. This study is particularly useful for the IRI community considering the fact that, since its establishment, the IRI model has continuously been improved and is still being updated as new data and more accurate models become available.

2. Data

Storm-time TEC considered as observations (GPS TEC) were derived from RINEX (Receiver INdependent EXchange) records using a software developed at Boston College (Seemala & Valladares, 2011), which allowed us to get both slant and vertical TEC (VTEC). For a specific time of the day, TEC values for different satellites were averaged to get TEC at that time. The cutoff satellite elevation angle was limited to 20° in order to reduce multipath effects. It is well known that during TEC derivation from GPS records, some errors are introduced. Possible sources of errors are due to instrumental biases, mapping function, and assumptions made during different steps involved in TEC derivation (Ho et al., 1997). The GPS TEC software used in this study reads the GPS raw data from RINEX files and calculates phase and code TEC values along with corresponding elevation and azimuth angles of the satellite(s) for the epochs and then estimates biases as briefly described in the following steps.

A single shell mapping function (Langley, 2002; Mannucci et al., 1993) is used to calculate the VTEC assuming an ionospheric pierce point height of 350 km (Rama Rao et al., 2006). Cycle slips in the phase TEC are corrected arithmetically by computing the difference between successive TEC values and comparing them with the mean difference of the last 20 values. This helps to reduce any noise at the start of data epoch or for low elevation angle. If the difference of the phase TEC at current epoch ($TECP_i$) to the previous value ($TECP_{i-1}$) is greater than 4 times the mean difference or 2 TEC units (TECUs) (considered for 30-s RINEX data), then the presence of a cycle slip (CS) is identified. The CS is then defined as $CS = TECP_i - TECP_{i-1} + \text{previous mean difference}$. And from the values there on, this cycle slip is corrected as $TECP_i = TECP_i - CS$.

After the cycle slip correction, the phase TEC is leveled to the code TEC to get absolute TEC without integer ambiguity. The differential satellite bias corrections published by University of Bern (<ftp://ftp.unibe.ch/aiub/CODE/>) are used to remove satellite biases. The differential receiver bias is assumed to be constant for the current data set (daily RINEX file data) and solved using the least squares method. A range

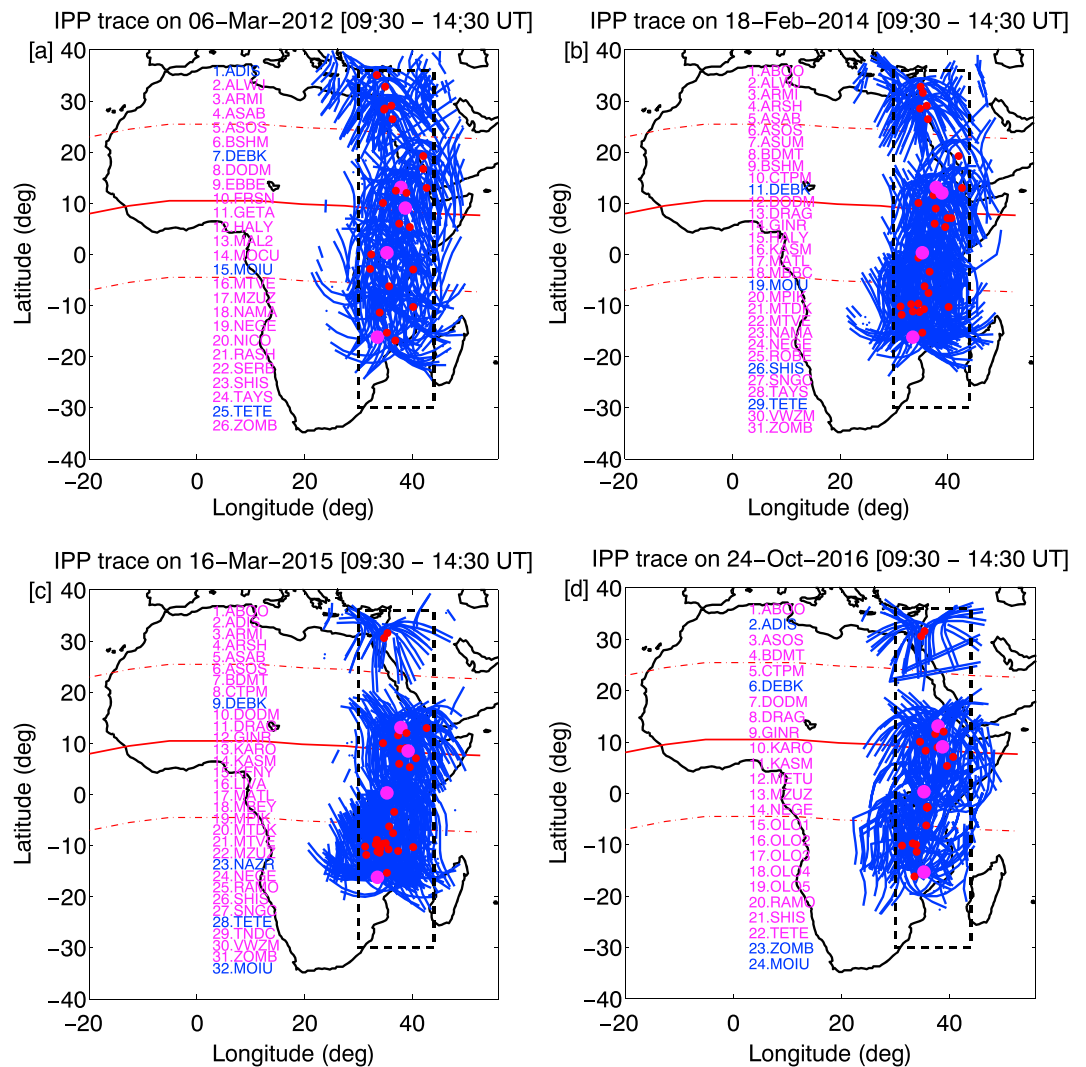


Figure 2. Global Positioning System ray traces at IPP altitude for five and a half hours worth of observation data, on (a) 6 March 2012, (b) 18 February 2014, (c) 16 March 2015, and (d) 24 October 2016. The Global Positioning System ground station code names (written in magenta and marked with smaller red dots) from which usable observation data for the inversion is obtained are listed along with the IPPs. Also, the stations whose code names are written in blue and marked as bigger dots (magenta) are used for validation only. The central time window is 12:00 UT. IPP = ionospheric pierce point.

of bias values for different satellites is added to the slant TEC (STEC), which is then used to calculate VTEC. Using the simple least squares method, the best bias value is selected. In this method, we check differences or error minimization using a range of possible bias values (e.g., from -300 to $+300$ TECUs in steps of 0.1 TECU), each of which is added to STEC and then VTEC is calculated. The resultant VTEC for the entire data set for this range of biases are checked for minimized difference against average diurnal TEC. The bias value that generated the minimum difference is then taken as the receiver bias for that day. The procedure is repeated for all days and final biases are added to STEC followed by the recalculation of final VTEC by the GPS TEC software. Figure 1 shows a typical example of the difference between calibrated (top panels) and uncalibrated (bottom panels) TEC over Nazret (NAZR, 8.57°N , 39.29°E , 0.25°S geomagnetic), Ethiopia, by taking into account cycle slips, satellite, and receiver biases for quiet (16 March 2015, Figure 1a) and disturbed (16 March 2015, Figure 1b) days, using an elevation threshold of 20° . The green and red curves represent VTEC from individual PRNs and the average TEC, respectively.

The GPS-TEC software used in this study has been compared with other techniques such as the one presented in Ciraoalo et al. (2007) along side the European Geostationary Navigation Overlay System (EGNOS) algorithm

Table 1

*Geographic (GLat & GLon) Coordinates and Magnetic Latitudes (MLA) of the Ground Receiver Stations Used for the Development (Showned With *) and Validation of ANN Models*

Station name	Station ID	Country	GLat (°)	GLon (°)	MLA (°)
Debarek	DEBK	Ethiopia	13.15	37.89	6.21
Sheb*	SHEB	Eritrea	15.85	39.05	9.71
Nazret*	NAZR	Ethiopia	8.57	39.29	0.78
Addis Ababa	ADIS	Ethiopia	9.04	38.77	1.28
Moiu*	MOIU	Kenya	0.29	35.29	−10.52
Tete*	TETE	Mozambique	−16.15	33.58	−33.01
Zomba	ZOMB	Malawi	−15.38	35.33	−31.45

which was taken as a reference (Abe et al., 2017). Generally, both softwares are consistent with EGNOS algorithm but the GPS-TEC software was found to be closer to EGNOS in low latitudes. On the other hand, the technique described in Ciruolo et al. (2007) was more accurate in mid latitudes, in estimating TEC derived from the EGNOS algorithm. It is worth noting that the same GPS-TEC software used in the current work has extensively been used to derive TEC in different studies that involved TEC computation (Adewale et al., 2011; Akala et al., 2013; Matamba et al., 2015; Olwendo et al., 2012; Seemala & Valladares, 2011).

For MIDAS, TEC reconstruction was done based on GPS measurements from receiver stations within -30° to 36° latitude and 30° to 44° longitude. The reason for selecting this region for the inversion technique is based on data availability that covers both African low latitude and midlatitude. Figure 2 shows the positions of GPS ground receiver stations used for the inversion (shown in small red dots) and GPS ray traces at the ionospheric pierce point (IPP) altitude of 350 km. Also listed for each storm period are code names of GPS receiver stations used for the inversion (magenta) and validation (blue). The GPS stations used for validation (listed in blue and shown with large magenta dots in Figure 2) were not used during the inversion to make validation data independent.

For TEC modeling, individual ANN models were developed based on historical storm-time TEC data, the storm criterion being $Dst \leq -50$ nT. Storm-time TEC data used to implement ANN models were derived from GPS measurements over receiver stations representing midlatitude: Tete (TETE, 16.15° S, 33.58° E; 26.94° S geomagnetic), Mozambique; low latitude: Moiu (MOIU, 0.29° N, 35.29° E; 9.17° S geomagnetic), Kenya; Nazret (NAZR, 8.57° N, 39.29° E, 0.25° S geomagnetic), Ethiopia; and Sheb (SHEB, 15.85° N, 39.05° E; 7.36° N geomagnetic), Eritrea. Due to the lack of data specifically for ANN model development, the African midlatitude in the northern hemisphere was not part of this study. Four geomagnetic storm periods were selected to evaluate MIDAS, ANN, and IRI capabilities to reconstruct/predict storm-time TEC. The selected validation periods were chosen in different stages of solar cycle: 6–13 March 2012 and 18–24 February 2014, 16–22 March 2015, and 24–30 October 2016, for high, moderate, and low solar activity periods, respectively. For independent validation data, the four validation storms periods were excluded in databases used to develop ANN models. In the case of missing data for some of the storm periods selected, the closest stations such as Addis Ababa (ADIS, 9.04° N, 38.77° E; 0.18° N geomagnetic), Ethiopia; Zomba (ZOMB, 15.38° S, 35.33° E; 26.07° S geomagnetic), Malawi; and Debarek (DEBK, 13.15° N, 37.89° E; 4.32° N geomagnetic), Ethiopia, were used for NAZR, TETE, and SHEB, respectively. Note that it has been demonstrated that a model developed at one station can be validated over any other location within a latitudinal and longitudinal coverage of 8.7° and 10.6° , respectively (Uwamahoro & Habarulema, 2015). Table 1 shows geographic coordinates and magnetic latitudes (MLAs) ($\tan(MLA) = 0.5 \times \tan I$) of GPS ground receiver stations considered to develop and validate ANN models. For each station, the magnetic inclination I used to compute MLA was obtained from the International Geomagnetic Reference Field model. Maximum K_p and minimum Dst values reached during the selected validation storm periods as well as the storm classification based on the National Oceanic and Atmospheric Administration Space Weather Scales available at <http://www.swpc.noaa.gov/noaa-scales-explanation> and according to Loewe and Prölss (1997) are presented in Table 2. For each station considered for validation, IRI TEC data were obtained by running the online IRI-2016 model available at https://omniweb.gsfc.nasa.gov/vitmo/iri2016_vitmo.html, with NeQuick as topside option and STORM option on. It is also important to mention that IRI model provides TEC values up to the altitude of 2,000 km (Chartier et al., 2012; Habarulema & Ssessanga, 2017).

Table 2

Classification of the Selected Storm Periods Based on K_p (NOAA Space Weather Scales) and Dst (Loewe & Pröls, 1997)

Storm period	Solar activity	Maximum K_p	Classification (NOAA)	Minimum Dst (nT)	Classification (Loewe & Pröls, 1997)
06–13 March 2012	High	8	Severe	–145	Strong
18–24 February 2014	High	6	Moderate	–116	Strong
16–22 March 2015	Moderate	8	Severe	–223	Severe
24–30 October 2016	Low	6	Moderate	–64	Moderate

Note. NOAA = National Oceanic and Atmospheric Administration.

3. TEC Reconstructing Techniques

3.1. MIDAS

Due to the dispersive nature of the ionosphere, dual-frequency radio signals transmitted from a GPS satellite experience differential phase changes, which are directly proportional to TEC between a satellite and receiver (Davies, 1990; Jayawardena et al., 2016; Yin et al., 2004). MIDAS is an inversion method that uses differential phase measurements of STEC as input data and computes the ionospheric electron density (Yin et al., 2004). For the ionospheric tomography, the region of the ionosphere that is required to be imaged is subdivided into three-dimensional elements, called *voxels*, which are bounded in latitude, longitude, and altitude (Bust et al., 2007; Mitchell & Spencer, 2003). In the current study, the African region within -30° to 36° latitude and 30° to 44° longitude was considered during inversion, with voxel elements defined by a grid of 2° latitude \times 2° longitude, and altitude range of 100 to 1,200 km in steps of 40 km. STEC used as input to MIDAS is an integrated quantity along the satellite-receiver signal path, and thus, ray path elements intercepting within a given voxel contain some plasmasphere contribution. It is therefore likely that an unknown amount of plasmaspheric TEC is included at ionospheric heights during reconstructions (Chartier et al., 2012; Kinrade, 2013). Since the matrix of ray path elements is rectangular and therefore can not be directly inverted, a set of orthonormal basis functions and an appropriate mapping matrix are required to perform the inversion (Mitchell & Spencer, 2003). The introduction of basis functions permits the representation of temporal and spatial distributions of the ionospheric electron density separately. The set of EOFs can be generated from ionospheric models such as IRI and Chapman functions (Mitchell & Spencer, 2003; Yin et al., 2017), and the latter was used in the current work. MIDAS uses observation data from a user-defined time window centered at the time of the inversion. However, depending on the choice of the length of the time window, which translates into the amount of observation data ingested in each time step of the inversion process, the final output may vary. Short temporal variations may not be captured when a wide time window is used but also the amount of observation data that goes into the inversion matters. Therefore, a compromise needs to be made between the amount of observation data that goes into a single run for a single solution and width of the time window. In a region of sparse GPS receivers such as the one considered in this study, shorter time windows mean less observation data for the inversion. Thus, observations from a sliding time window of 5.5 hr (shown in Figures 2a–2d) was used in the inversion to obtain electron densities at every 30 min interval. Also a nonlinear optimization method was used to produce the results presented in this study since it has an advantage of avoiding negative values of electron density. VTEC from MIDAS was computed by vertical integration of the electron density obtained following the above procedure. Detailed theory about MIDAS can be found in a number of literature sources (Bust et al., 2007; Jayawardena et al., 2016; Meggs et al., 2005; Mitchell & Spencer, 2003; Spencer & Mitchell, 2007; Yin et al., 2017) and references therein. For more information about the recent MIDAS algorithm used in this study, readers are referred to Spencer and Mitchell (2007), Giday et al. (2016), and Yin et al. (2017).

3.2. ANNs

In the context of modeling, presentation of known inputs and outputs to an ANN allows it to learn the underlying relationship between the two data sets and later generalizes to estimate the desired output (McKinnell & Poole, 2004; Oyeyemi et al., 2006). The information processing is performed within computational units called *neurons* or *nodes*, and signals are transmitted from one neuron to another through connection links (Fausett, 1994). For each connection link, there is an associated weight that strengthens inputs in such a way that the higher the weight multiplied by a given input, the stronger that input will be (Fausett, 1994). Each neuron is characterized by its internal state also known as its activation or activity level, which is defined as a function

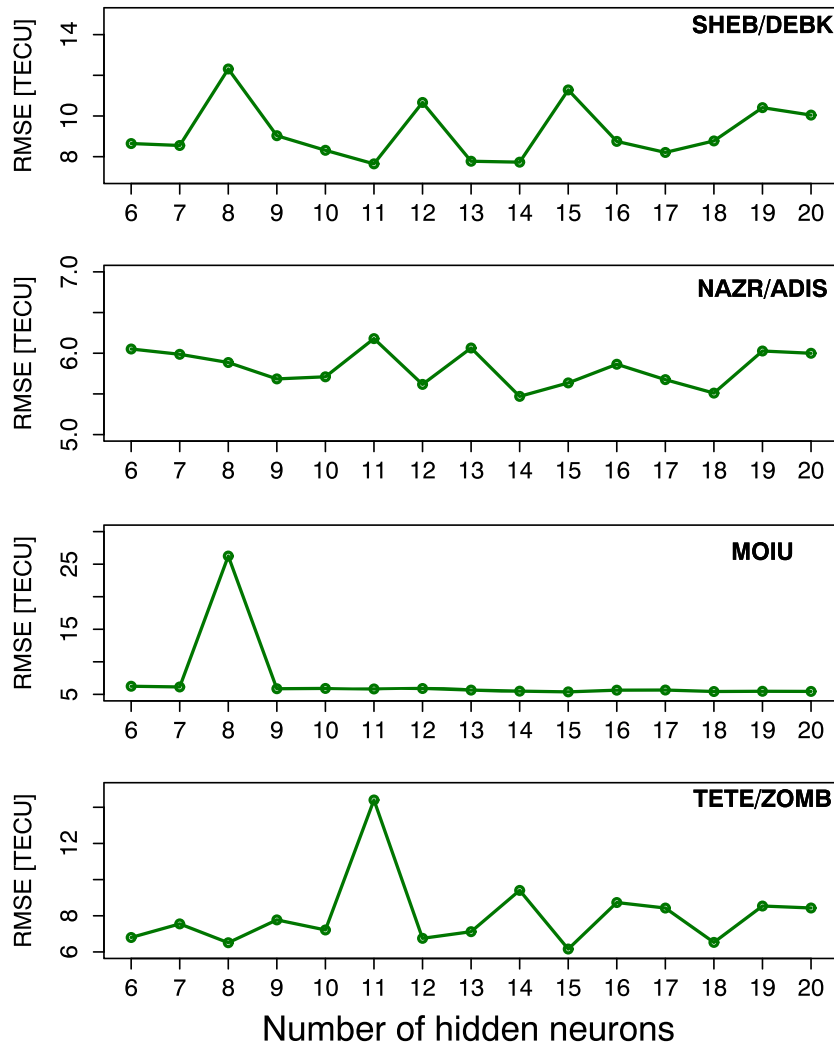


Figure 3. Variation of RMSE between Global Positioning System TEC observations and ANN predictions with number of hidden nodes for validation storm periods. RMSE = root-mean-square error; TEC = total electron content; ANN = artificial neural network.

of inputs received by that same neuron (Fausett, 1994). The main task of the activation function is to limit the amplitudes of the output signals of neurons (Haykin, 1994). When neurons are regarded as grouped in different layers, an ANN can have input, hidden, and output layers (Fausett, 1994; Haykin, 1994). Depending on the number of layers of connection links available in an ANN, the later is termed *single-layer* (one layer) or *multi-layer* (several layers; Fausett, 1994; Haykin, 1994). When there are no loops in an ANN, the information flow is performed in a forward direction, and thus, the output from one layer does not affect that same layer. Such a network is called *feed-forward neural network* (FFNN) (Fausett, 1994; Haykin, 1994).

The FFNN was used in the current TEC modeling. The selection of modeling inputs was done based on factors that influence TEC variability such as diurnal, seasonal, annual and semiannual variations, and solar and geomagnetic activities (Ercha et al., 2012; Habarulema et al., 2007). Diurnal variation is represented by time of the day t , while day number of the year d represents annual, semiannual, and seasonal variations of TEC. Previous studies (Habarulema et al., 2007; McKinnell & Poole, 2004; Oyeyemi et al., 2006; Poole & McKinnell, 2000) recommended that to achieve accurate results, the time of the day and day number of the year should be decomposed into cosine and sine components of time (tc , ts) and day (dc , ds) as follows:

$$tc = \cos\left(\frac{2\pi \times t}{24}\right), \quad ts = \sin\left(\frac{2\pi \times t}{24}\right) \quad (1)$$

$$dc = \cos\left(\frac{2\pi \times d}{365.25}\right), \quad ds = \sin\left(\frac{2\pi \times d}{365.25}\right). \quad (2)$$

Table 3
ANN Architectures, Data Coverage Periods, and Number of Data Points Within Data Sets Used to Develop ANN Models

Station	Architecture	Period	Number of data points
SHEB	8-11-1	2004–2016	178,946
NAZR	8-14-1	2007–2016	206,162
MOIU	8-15-1	2008–2016	224,491
TETE	8-15-1	2011–2016	178,258

The above decomposition also gets rid of unrealistic trends sometimes observed at midnight (Poole & McKinnell, 2000). Such unrealistic trends are not related to the physics around midnight but rather to inappropriate treatment of continuity at midnight. The solar activity was represented by the modified solar flux index $F_{10.7p} = (F_{10.7} + F_{10.7A})/2$, where $F_{10.7}$ is the daily solar flux index at a wavelength of 10.7 cm, and $F_{10.7A}$, the 81-day running mean of $F_{10.7}$. Planetary 3-hr *ap* index, auroral electrojet index *AE* (5-min time resolution), and the symmetric disturbance field in the horizontal component of the Earth's magnetic field *H* (5-min time resolution), *symH*, were all used during storm-time TEC modeling to globally represent different geomagnetic activity contributors to TEC variability at a latitudinal scale. The number of input neurons was therefore eight as defined by eight different inputs—*tc*, *ts*, *dc*, *ds*, *F107p*, *ap*, *AE*, and *symH*—whereas there was one output neuron corresponding to the modeled parameter, *TEC*. For a specific station, the ANN architecture used during training was determined by first selecting the number of hidden neurons that corresponds to the minimum error. This task was performed based on root-mean-square error (RMSE) defined by the formula

$$RMSE = \sqrt{\frac{1}{N} \sum_{i=1}^N (TEC_{rec} - TEC_{obs})^2} \quad (3)$$

where TEC_{rec} and TEC_{obs} are the reconstructed/predicted and observed TEC, respectively, and N is the number of observations. For each location, the network was trained by varying the number of hidden neurons from 6 to 20 (range selected randomly), followed by computation of the RMSE between the observed and the reconstructed/predicted TEC when ANN models are tested on validation data sets. Figure 3 illustrates the variation of RMSE with number of hidden neurons for different locations.

It is clear from Figure 3 that 15, 14, 11, and 15 hidden neurons were used for MOIU, NAZR/ADIS, SHEB/DEBK, and TETE/ZOMB, respectively, because they provided the lowest RMSE over the validation period. Therefore, the corresponding architectures (which gave minimum RMSE values) considered for TEC reconstruction by ANN are 8-15-1, 8-14-1, 8-11-1, and 8-15-1. The amount of data used for the development of ANN models and the fact that TEC varies with latitude differently, are likely the main reasons of different ANN architectures. Table 3 shows the selected architectures, data coverage periods, and number of data points within data sets used to develop ANN models.

FFNNs with Levenberg-Marquardt backpropagation algorithm were used during training in the current work. Such type of configuration is preferred especially the training algorithm that is well known for its time saving while implementing the input-output mapping process (Jang et al., 1997) and has previously been applied to quiet and storm-time TEC modeling over the South African midlatitude region (Habarulema & McKinnell, 2012; Uwamahoro & Habarulema, 2015).

4. Results

For each validation storm period the intensity and the occurrence time of the storm are shown by *Dst* and *Kp* indices. Figure 4 shows validation results from MIDAS, ANN, and IRI-2016 models along with GPS TEC observations for storms that occurred during high solar activity period, between 06 and 13 March 2012. The last panel of Figure 4 shows *Dst* and *Kp* indices, which indicate that the 6–13 March 2012 storm period consisted of a succession of storms with different intensities. For the entire storm period and for all stations, MIDAS reconstructs the storm-time TEC well and short-term features are accurately captured. Similarly, ANN model reconstructed TEC well for almost the entire storm period except some overestimations observed during daytime on 8 March 2012 for DEBK, ADIS, and MOIU. In contrast to what was observed for MIDAS and ANNs, IRI

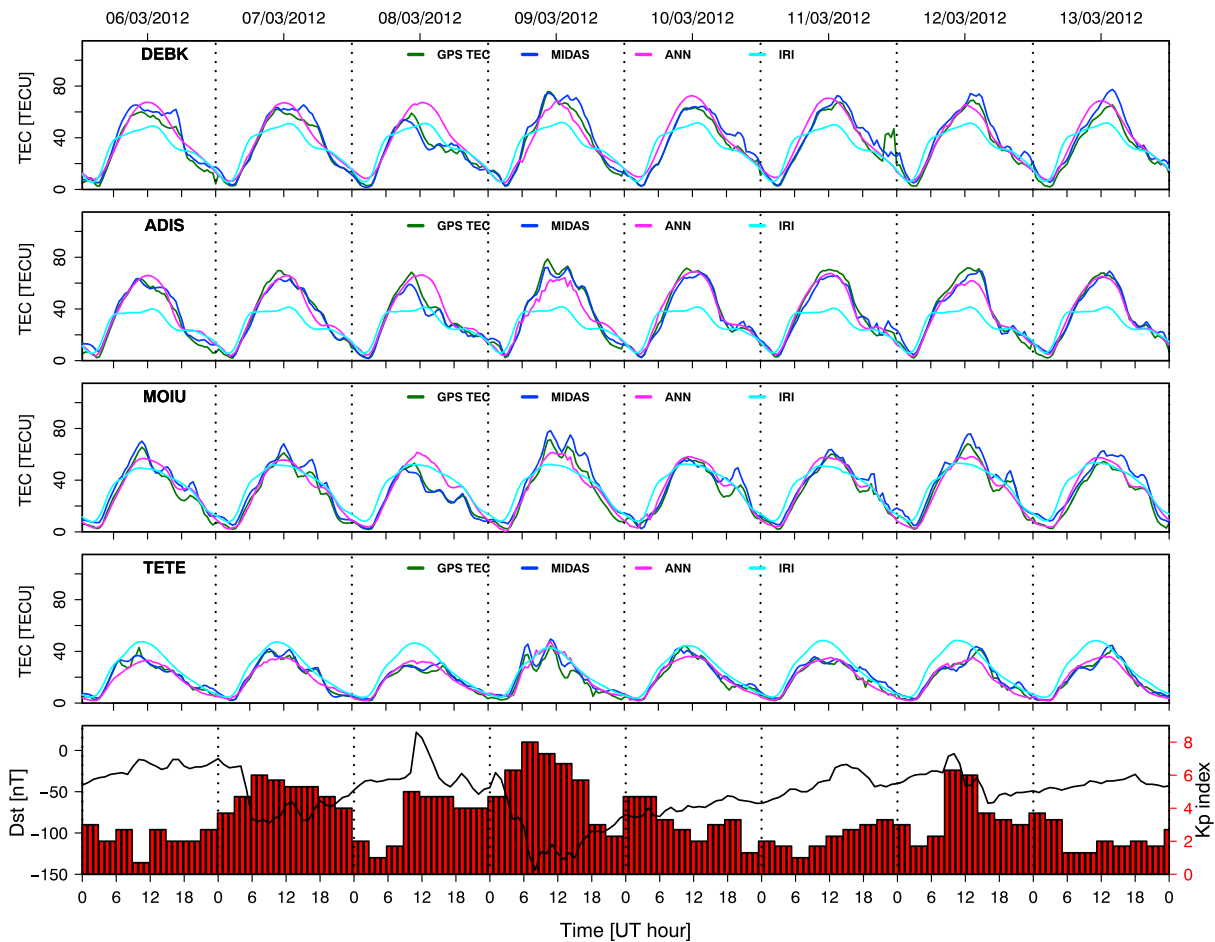


Figure 4. Comparison of the observed and reconstructed TEC for the storm period of 6–13 March 2012. GPS = Global Positioning System; TEC = total electron content; ANN = artificial neural network; MIDAS = Multi-Instrument Data Analysis System.

model shows large daytime underestimations of GPS TEC for the entire storm period specifically for DEBK and ADIS. While for DEBK and ADIS the RMSE values between IRI predictions and observations are about 9.83 and 15.69 TECU, IRI model provides more accurate predictions for MOIU and TETE with respective RMSE values of 8.77 and 8.17 TECU. However, some discrepancies dominated by underestimations and overestimations for MOIU and TETE, respectively, are observed specifically during daytime.

Figure 5 is similar to Figure 4 but for the storm period of 18–24 February 2014 and stations DEBK, NAZR, MOIU, and TETE. The 18–24 February 2014 storm period consisted of a sequence of storms as indicated by $Kp \geq 4$ or $Dst \leq -50$ nT. It can be seen from Figure 5 that MIDAS TEC agrees well with observations for NAZR and TETE. However, remarkable discrepancies mainly dominated by daytime overestimations are seen for DEBK and MOIU. What can also be noticed is the MIDAS good capability to capture short-term variations of the observed TEC and follow the TEC depletion over MOIU on 20 February 2014. ANN model estimates the observed TEC accurately in spite of some clear deviations on 19 February 2014 for DEBK, NAZR, and MOIU and on 23 February 2014 for DEBK. Except on 20 February 2014 where a good performance of IRI model in estimating the storm-time TEC magnitude is noticed for TETE and MOIU, IRI underestimates daytime TEC magnitude for the entire storm period.

Figure 6 presents MIDAS, ANN, and IRI results along with observations over DEBK, NAZR, MOIU, and TETE stations during the storm period of 16–22 March 2015. As indicated by the minimum Dst (-223 nT) and maximum Kp (of about 8) indices, the 16–22 March 2015 storm period consisted of one severe storm. The storm had a very long recovery phase that lasted for about 5 days as shown by Dst index below -50 nT for a prolonged time. Both MIDAS and ANNs reconstruct TEC accurately over all stations although for some days, daytime overestimations and underestimations are observed for DEBK and MOIU. TEC enhancement observed over

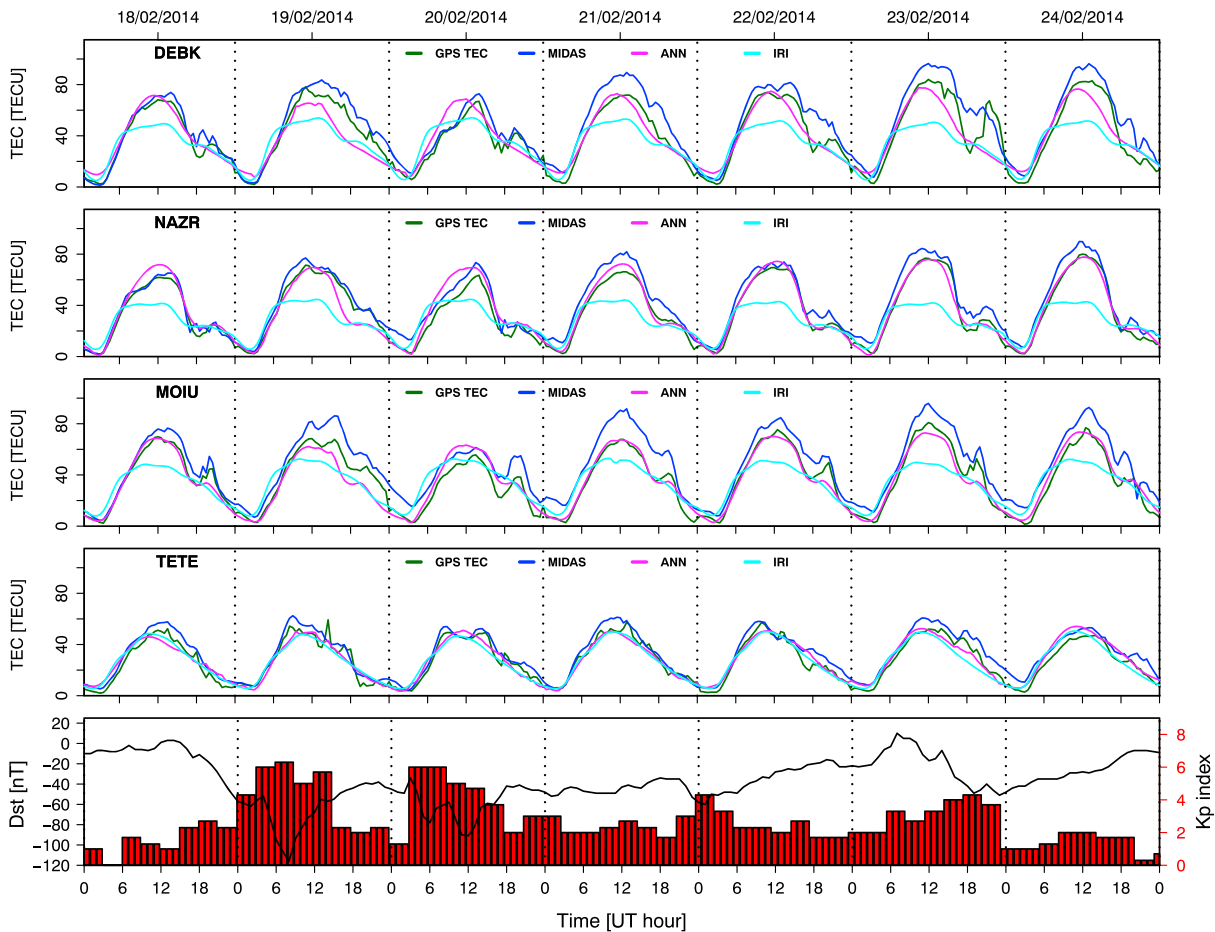


Figure 5. Comparison of the observed and reconstructed TEC for the storm period of 18–24 February 2014. GPS = Global Positioning System; TEC = total electron content; ANN = artificial neural network; MIDAS = Multi-Instrument Data Analysis System.

TETE on 17 March 2015 is well followed by MIDAS when compared with ANNs. The IRI model mainly underestimates TEC during daytime for the entire storm period for DEBK and NAZR and some days for MOIU, while relatively small overestimations are observed over TETE.

What is illustrated in Figure 7 are GPS TEC observations over DEBK, ADIS, MOIU, and ZOMB stations along with MIDAS, ANN, and IRI results, for a sequence of moderate geomagnetic storms that occurred between 24 and 30 October 2016. Except on 30 October 2016 where daytime overestimation is observed, MIDAS makes accurate estimations of TEC for DEBK, MOIU, and ZOMB for the rest of the storm period. The TEC depletion observed on 26 October 2016 over DEBK, MOIU, and ZOMB is also well captured by MIDAS. However, MIDAS underestimates daytime TEC over ADIS for almost the entire storm period. On the other hand, ANN model estimates the magnitude of TEC accurately for DEBK and MOIU but fails to capture the depletion observed on 26 October 2016. For ADIS and ZOMB, daytime TEC is underestimated for almost the entire storm period. Except on 26 October 2016 where the TEC depletion observed over the four stations is not seen by the IRI model, for the rest of the storm duration IRI predictions are in good agreement with observations specifically for DEBK and MOIU. However, for ADIS, daytime TEC magnitude is underestimated for some days, while for ZOMB an overestimation is observed throughout the storm period. The common characteristics for the three methods used for storm-time TEC reconstructions are their high accuracy in early morning and sometimes around midnight hours, and where overestimations/underestimations exist, these are generally observed during daytime.

To be able to determine which model/technique between MIDAS, ANNs, or IRI does better in reconstructing the storm-time TEC over different African latitude regions, a statistical analysis was done based on the mean absolute error (MAE) and Pearson’s correlation coefficient between the observed and reconstructed

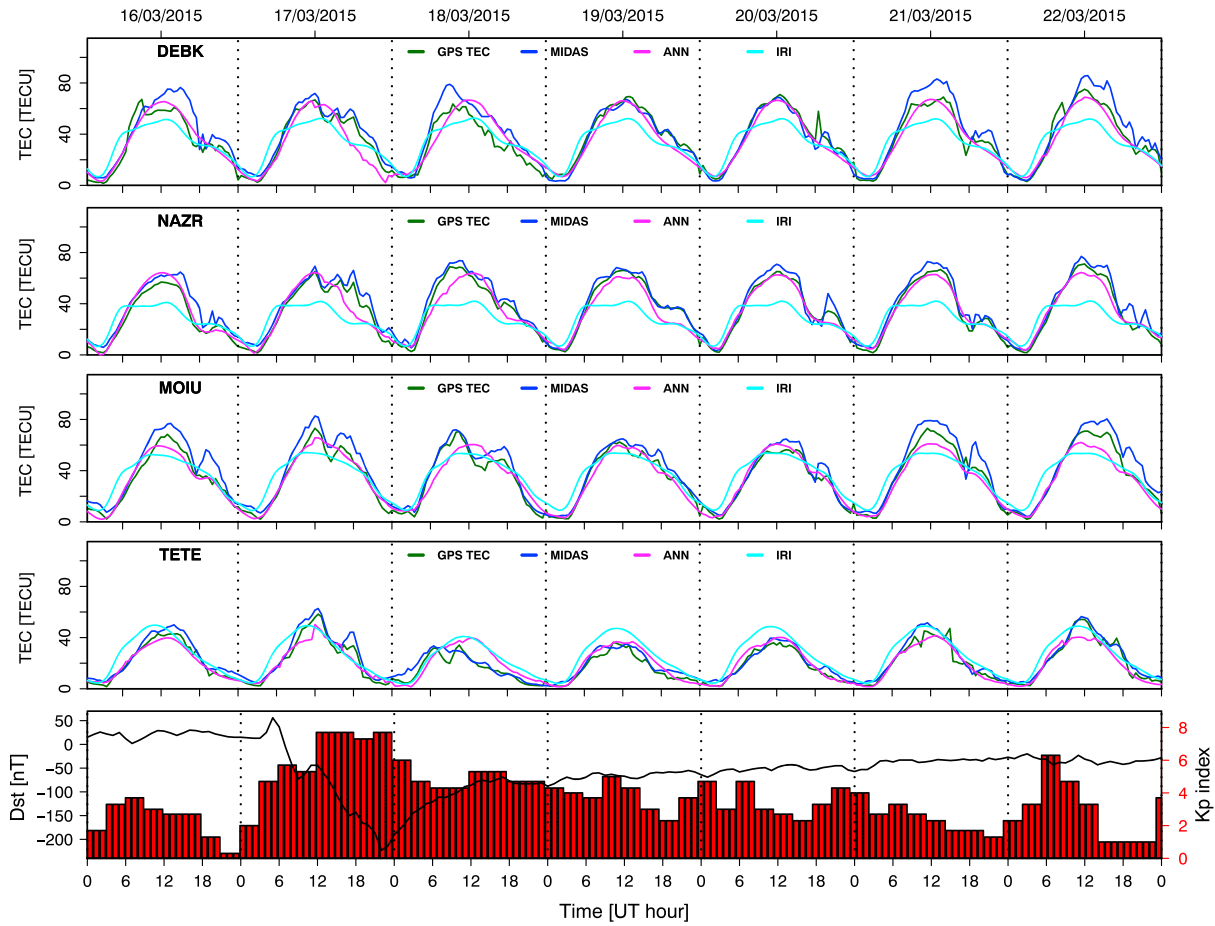


Figure 6. Comparison of the observed and reconstructed TEC for the storm period of 16–22 March 2015. GPS = Global Positioning System; TEC = total electron content; ANN = artificial neural network; MIDAS = Multi-Instrument Data Analysis System.

TEC. Starting from the definition of the absolute error (AE; Habarulema et al., 2007; Leandro & Santos, 2007):

$$AE = |TEC_{rec} - TEC_{obs}|, \quad (4)$$

MAE is given by (Mitchell & Spencer, 2003; Willmott & Matsuura, 2005)

$$MAE = \frac{1}{N} \sum_{i=1}^N |TEC_{rec} - TEC_{obs}| \quad (5)$$

where N is the number of observations. MAE represents the average of the vertical distances between the observed and predicted quantities and has been proven to be a good parameter to use over the RMSE in assessing the performance of a model (Willmott & Matsuura, 2005). Correlation coefficients were computed using the following formula in Suhov and Kelbert (2005):

$$R = \frac{cov(TEC_{obs}, TEC_{rec})}{\sigma_{obs}\sigma_{rec}} = \frac{\sum_{i=1}^N (TEC_{obs_i} - \overline{TEC_{obs}})(TEC_{rec_i} - \overline{TEC_{rec}})}{\sqrt{\sum_{i=1}^N (TEC_{rec_i} - \overline{TEC_{rec}})^2} \sqrt{\sum_{i=1}^N (TEC_{obs_i} - \overline{TEC_{obs}})^2}}. \quad (6)$$

where $cov(TEC_{obs}, TEC_{rec})$ represents the covariance between the observed (TEC_{obs}) and reconstructed TEC (TEC_{rec}), σ_{rec} and σ_{obs} are standard deviations of the reconstructed and observed TEC, respectively. TEC_{obs_i} and TEC_{rec_i} represent the i th observation and the corresponding reconstructed TEC, while $\overline{TEC_{obs}}$ and $\overline{TEC_{rec}}$ are the mean values of the observed and reconstructed TEC, respectively.

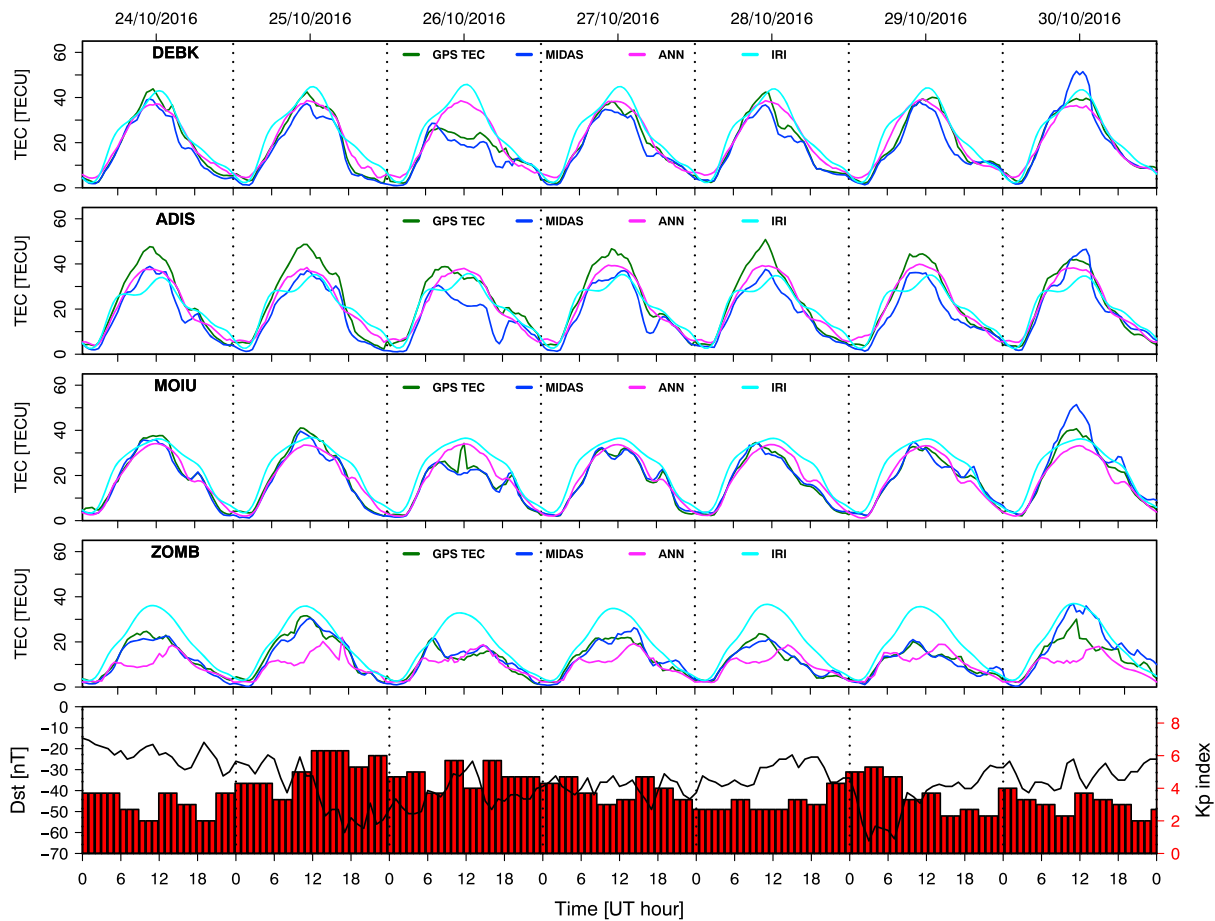


Figure 7. Comparison of the observed and reconstructed TEC for the storm period of 24–30 October 2016. GPS = Global Positioning System; TEC = total electron content; ANN = artificial neural network; MIDAS = Multi-Instrument Data Analysis System.

Figure 8 shows the calculated MAE values (left panels) and correlation coefficients (right panels) for all validation storm periods. For the storm periods of 6–13 March 2012 and 24–30 October 2016, smaller values of MAE generally found for MIDAS reveal that, on average, MIDAS reconstructs storm-time TEC better than ANN and IRI models. In contrast, for 18–24 February 2014 and 16–22 March 2015 storm periods, ANN model shows higher accuracy, on average. Except for TETE where MAE values for IRI model are comparable with the values obtained for ANNs specifically for the storm period of 18–24 February 2014, MAE values for IRI model are higher for all other cases. This indicates that IRI model is not as good as MIDAS and ANN techniques in making accurate storm-time TEC reconstructions. A similar observation was highlighted in previous works that compared MIDAS reconstructions with IRI predictions (Chartier et al., 2012; Giday et al., 2016), and ANN estimations with IRI predictions (Habarulema et al., 2007, 2009; Okoh et al., 2016; Watthanasangmechai et al., 2012). The underestimation of TEC by IRI model compared to MIDAS and ANN can be attributed to difference in altitude ranges TEC is estimated (Chartier et al., 2012; Habarulema & Ssessanga, 2017; Kenpankho et al., 2011). IRI model does generate TEC for the altitude range 60–2,000 km and the contribution of the plasmasphere is therefore not fully taken into account in IRI model. In contrast, it is worth noting that the input for MIDAS include GPS ray paths that contain information of the plasmasphere (Chartier et al., 2012). Similarly for ANNs, GPS TEC used to develop ANN models was derived based on the line integral of the electron density along the signal path from GPS satellites (at the altitude of about 20,200 km) to ground receivers. These may probably be some of the reasons that make MIDAS and ANNs more accurate in estimating the magnitude of TEC compared to IRI model. Particularly for ANN models, the amount of data used for training and the choice of the number of hidden nodes also influenced the modeling results. The fact that MIDAS captures short-term features and follows TEC enhancements and depletions observed during geomagnetic storms better than ANN and IRI models can be explained in terms of data used when applying or developing the techniques.

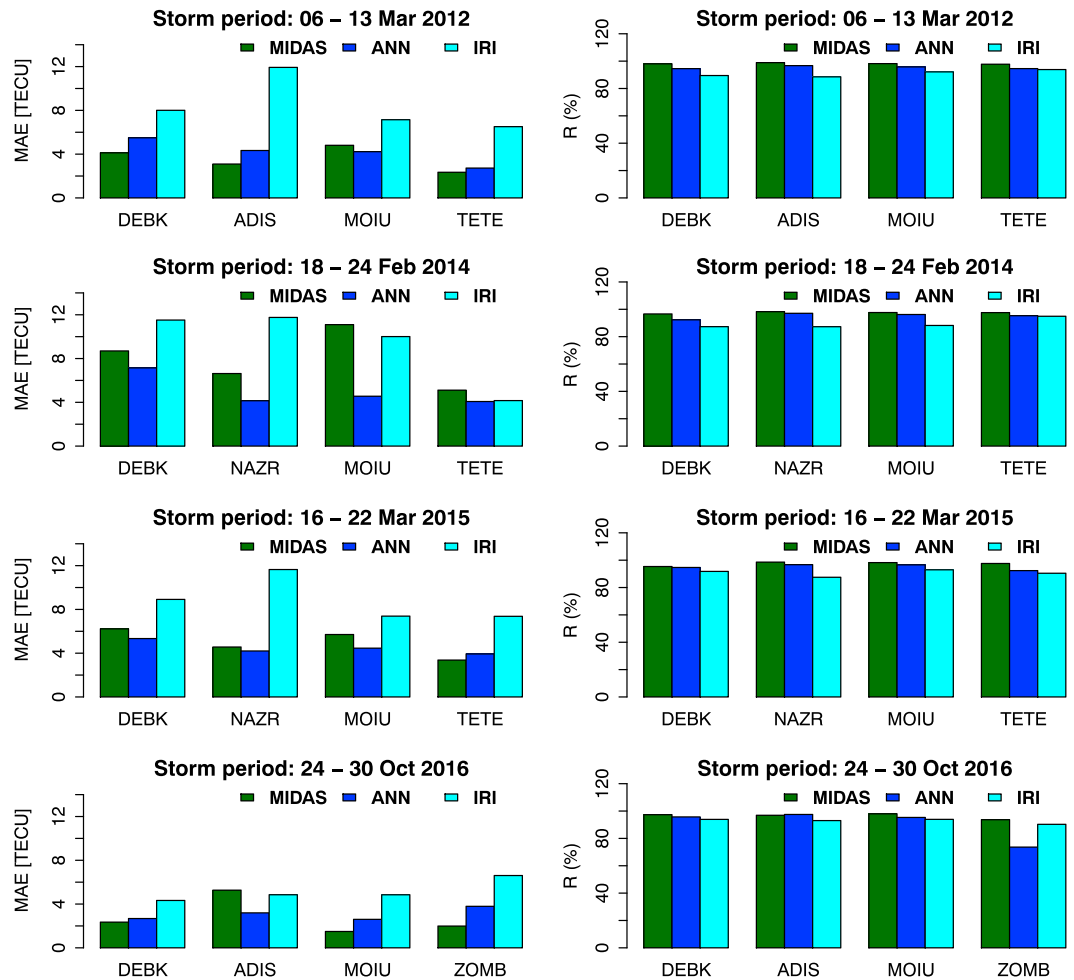


Figure 8. MAE and correlation between the observed and reconstructed TEC by MIDAS, ANN, and IRI. GPS = Global Positioning System; TEC = total electron content; ANN = artificial neural network; MIDAS = Multi-Instrument Data Analysis System; MAE = mean absolute error.

MIDAS uses direct measurements around the specific time of inversion/reconstruction, while ANNs and IRI are empirical models based on historical data.

It can also be seen from Figure 8 that relatively high values of MAE were generally found for the low-latitude stations (DEBK, NAZR, ADIS, and MOIU) compared to midlatitude stations (TETE and ZOMB). The average MAE values computed over the four validation storm periods per location (Table 4) confirm that higher error values were found for low latitudes. The reconstructing techniques used in this work estimate TEC better for the midlatitude than the low latitude. This agrees well with what was previously reported about the performance of IRI (Kumar et al., 2015) and MIDAS (Chartier et al., 2014) in low latitude and midlatitude. Generally, the difficulty in reconstructing/modeling the low-latitude ionosphere has been frequently reported (Adewale et al., 2011; Kenpankho et al., 2011; Materassi & Mitchell, 2005; Panda et al., 2015). Overall high values of MAE observed for the low latitude compared to midlatitude are likely due to higher TEC gradients caused by the equatorial ionisation anomaly as a result of the fountain effect. The influence of high TEC variability due to fountain effect on TEC modeling/reconstruction was reported as the major cause that makes modeling difficult for the low-latitude ionosphere. This observation was reported by Chartier et al. (2014) when performing the tomography of the African ionosphere during geomagnetically quiet conditions, and Panda et al. (2015) during TEC reconstruction with IRI model over low latitude in the Indian sector. It can therefore be considered that TEC reconstruction is more difficult for the low latitude than midlatitude and this agrees well with what was previously reported (Chartier et al., 2014; Kumar et al., 2015).

Table 4
Average Mean Absolute Error Values (in TECU) Computed Over Four Storm Periods for a Specific Station (First Three Columns) and Over All Stations Considered for Validation (Last Column)

Technique	DEBK	NAZR/ADIS	MOIU	TETE/ZOMB	Average over all stations
MIDAS	5.35	4.89	5.78	3.20	4.81
ANN	5.16	3.96	3.96	3.63	4.18
IRI	8.19	10.05	7.35	6.16	7.94

Note. MIDAS = Multi-Instrument Data Analysis System; ANN = artificial neural network; TEC = total electron content.

Owing to the assumptions in bias calculations, single shell mapping function used in conversion of STEC to VTEC (Mannucci et al., 1998), and computation of average TEC for all visible satellites at a specific time of the day, TEC accuracy in terms of standard deviation, is of the order of few TECUs (1–3 TECU) during geomagnetically quiet conditions, and this error may increase in disturbed conditions to about 3 to 6 TECU as demonstrated in Figure 9 with light-blue shaded areas. Figure 9 shows diurnal TEC over both midlatitude (SUTH, 32.38°S, 20.81°E) and equatorial latitude (ADIS, 9.04°S, 38.77°E) locations, for a disturbed day (9 March 2012) and the most quiet day of 25 March 2012. The average TEC is plotted in blue, while the shaded band within the red curves represents the range of standard deviation values. For ADIS and SUTH, it is clear that the error range is mostly between 1 and 3 TECU during quiet conditions (Figure 9, left panels) but also may increase during storm conditions up to 6 TECU as shown in Figure 9, particularly for SUTH (bottom right panel).

Different algorithms report varying values of observational errors partly due to the nature of treating different error sources. Using the TOPEX altimeter data as the “true” reference, Ho et al. (1997) reported RMSE of about 7 TECU between global ionospheric map products and TOPEX TEC within 1,000-km distance from the receivers during the geomagnetic storm period of 10–20 March 1993. Their analysis also showed that thin

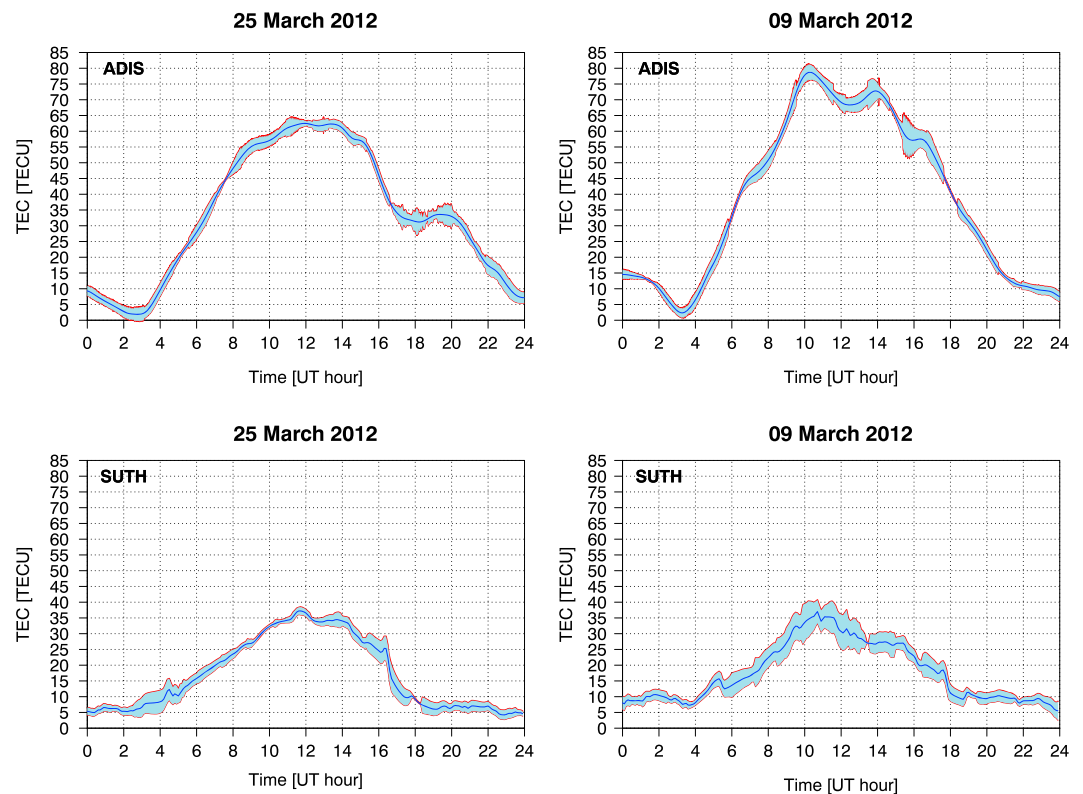


Figure 9. Diurnal vertical TEC (blue line) observed over midlatitude (SUTH, 32.38°S, 20.81°E) and equatorial latitude (ADIS, 9.04°S, 38.77°E) during quiet (25 March 2012, left panels) and disturbed (09 March 2012, right panels) days. The light-blue shaded areas represent the standard deviations of vertical TEC values for all visible satellites at a specific time of the day. TEC = total electron content.

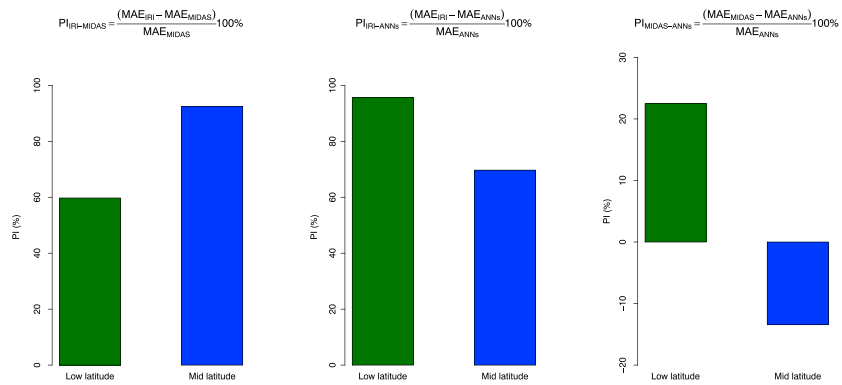


Figure 10. PI values for African low-latitude and midlatitude regions: IRI and MIDAS (left panel), IRI and ANNs (middle panel), and MIDAS and ANNs (right panel). Also shown above each panel are formulas used to compute PI values. MIDAS = Multi-Instrument Data Analysis System; ANN = artificial neural network; PI = percentage improvement.

shell approximation errors were significantly more in low latitudes compared to midlatitude regions that gave an error value of about 3 TECU during the same analyzed geomagnetically disturbed conditions. During quiet conditions, low-latitude RMSE value reduced to just over 3 TECU and the corresponding error for midlatitude was 2 TECU (Ho et al., 1997). Recently, Vierinen et al. (2016) developed a procedure of estimating Global Navigation Satellite System biases based on a comprehensive statistical framework and compared their results with TEC products at the MIT Haystack Observatory. They reported reduction in errors associated with TEC measurements from 2.25 to 1.60 TECU for 15 March 2015 and the new algorithm was less prone to outliers. A recent analysis by Abe et al. (2017) indicated that the average error (over low-latitude and midlatitude locations considered) between TEC estimates from the GPS-TEC software used in this study with respect to the values provided by the EGNOS algorithm considered as a reference is about 3 and 5 TECU for quiet and geomagnetically disturbed conditions, respectively. Therefore the reported MAE errors associated with ANN and MIDAS (Table 4) are either lower or in the same range of the typical TEC observation errors whereas MAE values determined from the IRI model are higher than 5 TECU for all the cases considered in this study. The ANN model can thus be used in providing TEC estimates in areas with insufficient GPS receiver coverage hence improving the performance of climatological models such as the IRI.

To evaluate how accurate a model performs with respect to another, the percentage improvement (*PI*) was computed according to the following equation (Muslim et al., 2015):

$$PI = \frac{MAE_1^{av} - MAE_2^{av}}{MAE_2^{av}} \times 100\% \quad (7)$$

where MAE_1^{av} and MAE_2^{av} are the average values of MAE for models 1 and 2, respectively. In the context of this work, models 1 and 2 represent any of MIDAS, ANNs, or IRI. Equation (7) indicates how much percentage model 2 performs better than model 1. Over the storm periods considered for validation, we found that, on average, ANN model performs 3.69%, 23.48%, and 45.96% better than MIDAS for DEBK, NAZR/ADIS, and MOIU, respectively. The average *PI* of 24.37% obtained for the three locations shows higher accuracy of ANN in the low latitude compared to MIDAS. The fact that individual storm-time ANN models were developed for different locations and not a regional model that covers the entire region of interest might be another contributing factor for the good performance of ANNs over MIDAS and IRI in the low-latitude ionosphere. However, we also note that a regional ANN model over the African region would be prone to significant errors due to few/lack of observations in some latitude regions. On the other hand, MIDAS performs better for the midlatitude station TETE/ZOMB by 13.44% compared to ANN model. Figure 10 illustrates *PI* values computed for African low-latitude and midlatitude regions. Since we have three locations (DEBK, NAZR/ADIS, and MOIU) that represented the low latitude in this study, average MAE over these locations was first calculated for each technique/model to represent the low latitude with a single value. Then the formulas presented in Figure 10 were applied to compute *PI* values for both low-latitude and midlatitude locations. Positive *PI* values shown on the left (IRI and MIDAS) and the middle (IRI and ANNs) panels of Figure 10 indicate that MIDAS and ANNs perform better than IRI for both low-latitude and midlatitude African regions. However, the right panel shows good performance of ANNs in low latitude compared to MIDAS, while a reverse situation is noticed in the midlatitude.

The high accuracy of ANN model in TEC modeling has previously been reported for both low-latitude (Acharya et al., 2011; Watthanasangmechai et al., 2012) and midlatitude regions (Huang & Yuan, 2014). Over all stations considered for validation, we wish to note that the average MAE values of 4.81, 4.18, and 7.94 TECU were found for MIDAS, ANN, and IRI, respectively. This confirms that, overall, MIDAS and ANN provide comparable results and are both better than IRI model for storm-time TEC reconstruction.

All three techniques considered in this work gave high correlation coefficients (between 73% and 99%). In the context of this study, high correlation coefficients confirm good performance of MIDAS, ANN, and IRI techniques in reproducing diurnal trend of the observed TEC. Over all stations, the highest correlation coefficients found for MIDAS indicate that there is a strong positive linear relationship between observations and MIDAS estimations compared to other techniques. It can therefore be concluded that MIDAS reconstructs short-term features and follows the storm-time TEC dynamics more accurately than IRI and ANN models. The high performance of MIDAS during disturbed conditions was noticed and reported by (Yin et al., 2004) when reconstructing the electron density over the United States. As it can be seen from Figure 8, there is no clear dependence of performances of MIDAS, ANNs, and IRI on the storm intensity. As an example, smaller MAE values were generally obtained for the severe storms of 16–22 March 2015 (minimum *Dst* of –223 nT) compared to strong storms of 18–24 February 2014 (minimum *Dst* of –116 nT).

5. Conclusion

We have statistically evaluated the capability of MIDAS compared with ANNs to reconstruct storm-time TEC for the African low-latitude and midlatitude regions. Based on geomagnetically disturbed conditions only, this study compared MIDAS, ANN, and IRI-2016 TEC reconstructions and validated the results with the real GPS TEC observations.

We have found that MIDAS and ANNs provide comparable results in reconstructing the storm-time TEC over different African latitudes with MAE values of 4.81 and 4.18 TECU, respectively. On the other hand, statistics show that, on average, ANN model performs 24.37% better than MIDAS in estimating storm-time TEC over low latitudes, while MIDAS accuracy is 13.44% higher than ANN in midlatitude. However, it has been shown that MIDAS captures short-term variations of the observed TEC and follows enhancements and depletions observed during geomagnetic storms more accurately than ANNs. Both MIDAS and ANN model provide more accurate storm-time TEC reconstructions than IRI model in African low-latitude and midlatitude regions.

Similar to previous studies (Chartier et al., 2014; Kumar et al., 2015; Panda et al., 2015), storm-time TEC reconstruction/modeling is more difficult for the low-latitude than midlatitude ionosphere. The fountain effect and the resulting higher TEC gradients over low-latitude ionosphere are likely to be the causes of the difficulty in reconstructing/modeling TEC over this region.

The performance of MIDAS, ANNs, and IRI do not seem to depend on the storm intensity. For example, it was shown that MIDAS, ANNs, and IRI can even reconstruct storm-time TEC more accurately for severe storms (e.g., 16–22 March 2015) than it does for strong storms (e.g., 18–24 February 2014).

Acknowledgments

We acknowledge the INVERT team of the University of Bath, UK, for the use of MIDAS. This work was funded by the South African National Research Foundation (NRF) and South African National Space Agency (SANSA). Data used can be found at the following sources: <https://www.unavco.org/data/data.html> and <http://www.igs.org/products> for GPS RINEX data; http://wdc.kugi.kyoto-u.ac.jp/dst_realtime/index.html for *Dst*; <https://omniweb.gsfc.nasa.gov/form/dx1.html> for a_p , K_p , and $F_{10.7}$ indices; and https://omniweb.gsfc.nasa.gov/form/omni_min.html, for 5 min resolution *AE* and *symH*.

References

- Abe, O., Villamide, X. O., Paparini, C., Radicella, S., Nava, B., & Rodríguez-bouza, M. (2017). Performance evaluation of GNSS-TEC estimation techniques at the grid point in middle and low latitudes during different geomagnetic conditions. *Journal of Geodesy*, *91*(4), 409–417.
- Acharya, R., Roy, B., Sivaraman, M., & Dasgupta, A. (2011). Prediction of ionospheric total electron content using adaptive neural network with in-situ learning algorithm. *Advances in Space Research*, *47*(1), 115–123.
- Adewale, A., Oyeyemi, E., Adeniyi, J., Adeloye, A., & Oladipo, O. (2011). Comparison of total electron content predicted using the IRI-2007 model with GPS observations over Lagos, Nigeria. *Indian Journal of Radio & Space Physics*, *40*, 21–25.
- Akala, A., Seemala, G., Doherty, P., Valladares, C., Carrano, C., Espinoza, J., & Oluyo, S. (2013). Comparison of equatorial GPS-TEC observations over an African station and an American station during the minimum and ascending phases of solar cycle 24. *Annales Geophysicae*, *31*(11), 2085–2096.
- Borries, C., Jakowski, N., & Wilken, V. (2009). Storm induced large scale TIDs observed in GPS derived TEC. *Annales Geophysicae*, *27*, 1605–1612.
- Bust, G., Crowley, G., Garner, T., Gaussiran, T., Meggs, R. W., Mitchell, C. N., et al. (2007). Four-dimensional GPS imaging of space weather storms. *Space Weather*, *5*, S02003. <https://doi.org/10.1029/2006SW000237>
- Cander, L. R. (1998). Artificial neural network applications in ionospheric studies. *Annals of Geophysics*, *41*(5-6).
- Chartier, A. T., Kinrade, J., Mitchell, C. N., Rose, J. A., Jackson, D. R., Cilliers, P., et al. (2014). Ionospheric imaging in Africa. *Radio Science*, *49*, 19–27. <https://doi.org/10.1002/2013RS005238>
- Chartier, A. T., Mitchell, C. N., & Jackson, D. R. (2012). A 12 year comparison of MIDAS and IRI 2007 ionospheric total electron content. *Advances in Space Research*, *49*(9), 1348–1355.
- Ciraolo, L., Azpilicueta, F., Brunini, C., Meza, A., & Radicella, S. (2007). Calibration errors on experimental slant total electron content (TEC) determined with GPS. *Journal of Geodesy*, *81*(2), 111–120.

- Davies, K. (1990). *Ionospheric radio*. London, United Kingdom: Peter Peregrinus Ltd.
- Dear, R. M., & Mitchell, C. N. (2006). GPS interfrequency biases and total electron content errors in ionospheric imaging over Europe. *Radio Science*, 41, RS6007. <https://doi.org/10.1029/2005RS003269>
- Ercha, A., Huang, W., Yu, S., Liu, S., Shi, L., Gong, J., et al. (2015). A regional ionospheric TEC mapping technique over China and adjacent areas on the basis of data assimilation. *Journal of Geophysical Research: Space Physics*, 120, 5049–5061. <https://doi.org/10.1002/2015JA021140>
- Ercha, A., Zhang, D., Ridley, A. J., Xiao, Z., & Hao, Y. (2012). A global model: Empirical orthogonal function analysis of total electron content 1999–2009 data. *Journal of Geophysical Research*, 117, A03328. <https://doi.org/10.1029/2011JA017238>
- Fausett, L. (1994). *Fundamentals of neural networks: Architectures, algorithms, and applications*. New Jersey: Prentice-Hall Inc.
- Fesen, C., Crowley, G., & Roble, R. (1989). Ionospheric effects at low latitudes during the March 22, 1979, geomagnetic storm. *Journal of Geophysical Research*, 94(A5), 5405–5417.
- Fuller-Rowell, T., Codrescu, M., Moffett, R., & Quegan, S. (1994). Response of the thermosphere and ionosphere to geomagnetic storms. *Journal of Geophysical Research*, 99(A3), 3893–3914.
- Giday, N. M., Katamzi, Z. T., & McKinnell, L.-A. (2016). Ionospheric tomography over South Africa: Comparison of MIDAS and ionosonde measurements. *Advances in Space Research*, 57(1), 245–256.
- Habarulema, J., & McKinnell, L.-A. (2012). Investigating the performance of neural network backpropagation algorithms for TEC estimations using South African GPS data. *Annales Geophysicae*, 30(5), 857–866.
- Habarulema, J. B., McKinnell, L.-A., Burešová, D., Zhang, Y., Seemala, G., Ngwira, C., et al. (2013). A comparative study of TEC response for the African equatorial and mid-latitudes during storm conditions. *Journal of Atmospheric and Solar-Terrestrial Physics*, 102, 105–114.
- Habarulema, J. B., McKinnell, L.-A., & Cilliers, P. J. (2007). Prediction of global positioning system total electron content using neural networks over South Africa. *Journal of Atmospheric and Solar-Terrestrial Physics*, 69(15), 1842–1850.
- Habarulema, J. B., McKinnell, L.-A., Cilliers, P. J., & Opperman, B. D. (2009). Application of neural networks to South African GPS TEC modelling. *Advances in Space Research*, 43(11), 1711–1720.
- Habarulema, J. B., McKinnell, L.-A., & Opperman, B. D. (2010). TEC Measurements and modelling over Southern Africa during magnetic storms; a comparative analysis. *Journal of Atmospheric and Solar-Terrestrial Physics*, 72(5-6), 509–520.
- Habarulema, J. B., & Ssessanga, N. (2017). Adapting a climatology model to improve estimation of ionosphere parameters and subsequent validation with radio occultation and ionosonde data. *Space Weather*, 15, 84–98. <https://doi.org/10.1002/2016SW001549>
- Haykin, S. (1994). *Neural networks. A comprehensive foundation*. New York: Macmillan College Publishing Company.
- Ho, C., Wilson, B., Mannucci, A., Lindqwister, U., & Yuan, D. (1997). A comparative study of ionospheric total electron content measurements using global ionospheric maps of GPS, TOPEX radar, and the Bent model. *Radio Science*, 32(4), 1499–1512.
- Huang, Z., & Yuan, H. (2014). Ionospheric single-station TEC short-term forecast using RBF neural network. *Radio Science*, 49, 283–292. <https://doi.org/10.1002/2013RS005247>
- Jang, J.-S. R., Sun, C.-T., & Mizutani, E. (1997). *Neuro-fuzzy and soft computing; A computational approach to learning and machine intelligence*. United States of America: Prentice-Hall.
- Jayawardena, P., Talini, S., Chartier, A. T., Spencer, P., & Mitchell, C. N. (2016). Imaging the topside ionosphere and plasmasphere with ionospheric tomography using COSMIC GPS TEC. *Journal of Geophysical Research: Space Physics*, 121, 817–831. <https://doi.org/10.1002/2015JA021561>
- Katamzi, Z. T., & Habarulema, J. B. (2014). Traveling ionospheric disturbances observed at South African midlatitudes during the 29–31 October 2003 geomagnetically disturbed period. *Advances in Space Research*, 53(1), 48–62.
- Kenpankho, P., Watthanasangmechai, K., Supnithi, P., Tsugawa, T., & Maruyama, T. (2011). Comparison of GPS TEC measurements with IRI TEC prediction at the equatorial latitude station, Chumphon, Thailand. *Earth, Planets and Space*, 63(4), 365–370.
- Kinrade, J. (2013). Ionospheric imaging and scintillation monitoring in the Antarctic and Arctic, (PhD thesis). Bath, UK: University of Bath.
- Kumar, S., Tan, E. L., & Murti, D. S. (2015). Impacts of solar activity on performance of the IRI-2012 model predictions from low to mid latitudes. *Earth, Planets and Space*, 67(1), 1–17.
- Langley, R. (2002). Mapping the low-latitude ionosphere with GPS. *GPS World*, 13(2), 41–47.
- Leandro, R., & Santos, M. (2007). A neural network approach for regional vertical total electron content modelling. *Studia Geophysica et Geodaetica*, 51(2), 279–292.
- Loewe, C. A., & Prölss, G. W. (1997). Classification and mean behavior of magnetic storms. *Journal of Geophysical Research*, 102(A7), 14,209–14,213.
- Ma, X., Maruyama, T., Ma, G., & Takeda, T. (2005). Three-dimensional ionospheric tomography using observation data of GPS ground receivers and ionosonde by neural network. *Journal of Geophysical Research*, 110, A05308. <https://doi.org/10.1029/2004JA010797>
- Mannucci, A. J., Wilson, B. D., & Edwards, C. D. (1993). A new method for monitoring the Earth's ionospheric total electron content using the GPS global network. In *Proceedings of the 6Th International Technical Meeting of the Satellite Division of the Institute of Navigation (ION GPS 1993)* (pp. 1323–1332). Salt Lake City, UT.
- Mannucci, A., Wilson, B., Yuan, D., Ho, C., Lindqwister, U., & Runge, T. (1998). A global mapping technique for GPS-derived ionospheric total electron content measurements. *Radio Science*, 33(3), 565–582.
- Maruyama, T. (2007). Regional reference total electron content model over Japan based on neural network mapping techniques. *Annales Geophysicae*, 25(12), 2609–2614.
- Matamba, T. M., Habarulema, J. B., & McKinnell, L.-A. (2015). Statistical analysis of the ionospheric response during geomagnetic storm conditions over South Africa using ionosonde and GPS data. *Space Weather*, 13, 536–547. <https://doi.org/10.1002/2015SW001218>
- Materassi, M., & Mitchell, C. N. (2005). Imaging of the equatorial ionosphere. *Annals of Geophysics*, 48(3), 477–482.
- McKinnell, L.-A., & Poole, A. W. (2004). Predicting the ionospheric F layer using neural networks. *Journal of Geophysical Research*, 109, A08308. <https://doi.org/10.1029/2004JA010445>
- Meggs, R. W., Mitchell, C. N., & Howells, V. (2005). Simultaneous observations of the main trough using GPS imaging and the EISCAT radar. *Annales Geophysicae*, 23(3), 753–757.
- Mitchell, C. N., & Spencer, P. S. (2003). A three-dimensional time-dependent algorithm for ionospheric imaging using gps. *Annals of Geophysics*, 46(4), 687–696.
- Muella, M. T., de Paula, E. R., Mitchell, C. N., Kintner, P. M., Paes, R. R., & Batista, I. S. (2011). Tomographic imaging of the equatorial and low-latitude ionosphere over central-eastern Brazil. *Earth, Planets and Space*, 63(2), 129–138.
- Muslim, B., Haralambous, H., Oikonomou, C., & Anggarani, S. (2015). Evaluation of a global model of ionospheric slab thickness for f_oF_2 estimation during geomagnetic storm. *Annals of Geophysics*, 58(5), A0551.
- Okoh, D., Owolabi, O., Ekechukwu, C., Folarin, O., Arhiwo, G., Agbo, J., et al. (2016). A regional GNSS-VTEC model over Nigeria using neural networks: A novel approach. *Geodesy and Geodynamics*, 7(1), 19–31.

- Olwendo, O., Baki, P., Mito, C., & Doherty, P. (2012). Characterization of ionospheric GPS total electron content (GPS TEC) in low latitude zone over the Kenyan region during a very low solar activity phase. *Journal of Atmospheric and Solar-Terrestrial Physics*, *84*, 52–61.
- Oyeyemi, E. O., McKinnell, L., & Poole, A. (2006). Near-real time f_oF_2 predictions using neural networks. *Journal of Atmospheric and Solar-Terrestrial Physics*, *68*(16), 1807–1818.
- Panda, S., Gedam, S., & Rajaram, G. (2015). Study of ionospheric TEC from GPS observations and comparisons with IRI and SPIM model predictions in the low latitude anomaly indian subcontinental region. *Advances in Space Research*, *55*(8), 1948–1964.
- Poole, A. W., & McKinnell, L.-A. (2000). On the predictability of f_oF_2 using neural networks. *Radio Science*, *35*(1), 225–234.
- Pröls, G. (1980). Magnetic storm associated perturbations of the upper atmosphere: Recent results obtained by satellite-borne gas analyzers. *Reviews of Geophysics*, *18*(1), 183–202.
- Rama Rao, P. R., Niranjana, K., Prasad, D., Krishna, S. G., & Uma, G. (2006). On the validity of the ionospheric pierce point (IPP) altitude of 350 km in the Indian equatorial and low-latitude sector. *Annales Geophysicae*, *24*(8), 2159–2168.
- Ratnam, D. V., Dinesh, B. V., Tejaswi, B., Kumar, D. P., Ritesh, T., Brahmanadam, P., & Vindhya, G. (2012). TEC Prediction model using neural networks over a low latitude GPS station. *International Journal of Soft Computing and Engineering (IJSCSE)*, *2*, 517–521.
- Rose, J. A., Watson, R. J., Allain, D. J., & Mitchell, C. N. (2014). Ionospheric corrections for GPS time transfer. *Radio Science*, *49*, 196–206. <https://doi.org/10.1002/2013RS005212>
- Seemala, G., & Valladares, C. (2011). Statistics of total electron content depletions observed over the South American continent for the year 2008. *Radio Science*, *46*, RS5019. <https://doi.org/10.1029/2011RS004722>
- Spencer, P. S., & Mitchell, C. N. (2007). Imaging of fast moving electron-density structures in the polar cap. *Annals of Geophysics*, *50*(3), 427–434.
- Suhov, Y., & Kelbert, M. (2005). *Probability and statistics by example, volume I. Basic probability and statistics*. Cambridge, UK: Cambridge University Press.
- Tsurutani, B., Mannucci, A., Iijima, B., Abdu, M. A., Sobral, J. H. A., Gonzalez, W., et al. (2004). Global dayside ionospheric uplift and enhancement associated with interplanetary electric fields. *Journal of Geophysical Research*, *109*, A08302. <https://doi.org/10.1029/2003JA010342>
- Tsurutani, B., Saito, A., Verkhoglyadova, O., Mannucci, A., Abdu, M., Araki, T., et al. (2006). The dayside ionospheric “superfountain” (DIS), plasma transport and other consequences. In *Proceedings of the ILWS Workshop*. Goa, India.
- Tulunay, E., Senalp, E. T., Cander, L. R., Tulunay, Y. K., Bilge, A. H., Mizrahi, E., et al. (2004). Development of algorithms and software for forecasting, nowcasting and variability of TEC. *Annals of Geophysics*, *47*(2-3), 1201–1214.
- Uwamahoro, J. C., & Habarulema, J. B. (2015). Modelling total electron content during geomagnetic storm conditions using empirical orthogonal functions and neural networks. *Journal of Geophysical Research: Space Physics*, *120*, 11,000–11,012. <https://doi.org/10.1002/2015JA021961>
- Vierinen, J., Coster, A. J., Rideout, W. C., Erickson, P. J., & Norberg, J. (2016). Statistical framework for estimating GNSS bias. *Atmospheric Measurement Techniques*, *32*(9), 1303–1312.
- Watthanasangmechai, K., Supnithi, P., Lerkvaranyu, S., Tsugawa, T., Nagatsuma, T., & Maruyama, T. (2012). TEC Prediction with neural network for equatorial latitude station in Thailand. *Earth, Planets and Space*, *64*(6), 473–483.
- Willmott, C. J., & Matsuura, K. (2005). Advantages of the mean absolute error (MAE) over the root mean square error (RMSE) in assessing average model performance. *Climate Research*, *30*(1), 79–82.
- Yin, P., Mitchell, C. N., Spencer, P. S., & Foster, J. C. (2004). Ionospheric electron concentration imaging using GPS over the USA during the storm of July 2000. *Geophysical Research Letters*, *31*, L12806. <https://doi.org/10.1029/2004GL019899>
- Yin, P., Zheng, Y.-N., Mitchell, C. N., & Li, B. (2017). A multi-resolution inversion for imaging the ionosphere. *Journal of Geophysical Research: Space Physics*, *122*, 6799–6811. <https://doi.org/10.1002/2016JA023728>